# Journal of Materials Chemistry A

Accepted Manuscript



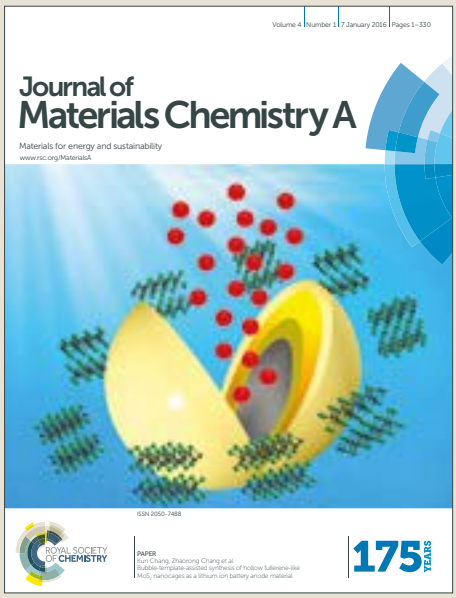




ROYAL SOCIETY OF CHEMISTRY

rsc.li/materials-a

View Article Online
DOI: 10.1039/C6TA10739G

Journal Materials Chemistry A

ARTICLE



# Bis(tri-n-alkylsilyl oxide) silicon phthalocyanines: A Start to Establishing a Structure Property Relationship as both Ternary Additives and Non-Fullerene Electron Acceptors in Bulk Heterojunction Organic Photovoltaic Devices.

Received 00th January 20xx,
Accepted 00th January 20xx

DOI: 10.1039/x0xx00000x

www.rsc.org/

Minh-Trung Dang,[a,†] Trevor M. Grant,[a,c†] Han Yan[b], Dwight S. Seferos[b], Benoît H. Lessard,[a,c,*] and Timothy P. Bender*[,a,b,d]

Previous studies have shown that the use of bis(tri-*n*-hexylsilyl oxide) silicon phthalocyanine ((3HS)$_2$-SiPc) as a solid ternary electroactive additive in poly(3-hexylthiophene):phenyl-C$_{61}$-butyric acid methyl ester P3HT:PC$_{61}$BM bulk heterojunction organic photovoltaic (BHJ OPV) devices resulted in an increased performance. It has been hypothesized that the increase in efficiency is partially due to the unique and odd combination of high solubility and strong driving force of crystallize previously observed for (3HS)$_2$-SiPc. In this follow up study, two chemical variants of (3HS)$_2$-SiPc, bis(tri-*n*-butylsilyl oxide) ((3BS)$_2$-SiPc) and bis(tri-*n*-isopropylsilyl oxide) ((3TS)$_2$-SiPc) were synthesized to determine how small changes in chemical structure would affect the properties of the material and its performance within BHJ OPV devices. We observed that the use of either (3XS)$_2$-SiPc compound results in a further ~10% increase in *Jsc* compared to the use of (3HS)$_2$-SiPc. We also did a preliminary assessment of the use of the three (3XS)$_2$-SiPcs as replacements for PC$_{61}$BM in straight binary P3HT-based BHJ OPV devices. Despite achieving only ~1% PCE efficiencies, observations including a ≈ 50% increase in $V_{OC}$ over a P3HT:PC$_{61}$BM baseline and a decent fill factor indicate to us that (3XS)$_2$-SiPcs do have potential as non-fullerene acceptors and advantageous alternatives due to their low embedded energy and therefore their inherent sustainability. X-ray diffraction of ternary and binary BHJ devices demonstrate that both (3BS)$_2$-SiPc and (3TS)$_2$-SiPc experienced similar increase in crystallite density (d-spacing) relative to (3HS)$_2$-SiPc which we surmise plays a role in the improved device efficiency. Like (3HS)$_2$-SiPc, for these two new additives, we also observed a high tendency to crystallize. The results from this study suggest that solubility and driving force to crystalize are important factors in determining the extent to which an additive will migrate to the donor/acceptor interface and thus affect its performance as a ternary additive in BHJ OPV device. Based on the three (3XS)$_2$-SiPcs used in this study, the smaller tri-n-alkylsilyl oxide molecular fragments seem to work better. Therefore, moving forward, we will continue to consider smaller molecular fragments that still enable solubility and processability of (3XS)$_2$-SiPcs.

## Introduction

Increased interest in solar energy capture has seen a strong growth in solar cell research over the past decade. There are also continuing research efforts to provide an inexpensive source of renewable energy capture with limited embedded energy within the device.[1] Among other solar collectors, organic photovoltaic (OPV) devices show great promise due to their potential for inexpensive processing and short energy payback time compared to silicon based devices.[1] Bulk heterojunction (BHJ) OPV devices are among the most studied, where the active layer is most often composed of a blend of an electron donating conjugated polymer and a fullerene based electron accepting small molecule.[1] Poly(3-hexylthiophene) (P3HT) and phenyl-C$_{61}$-butyric acid methyl ester (PC$_{61}$BM) are by far the most studied donor / acceptor paired materials for use as an active layer within the BHJ OPV space, with baseline PCEs ranging from 2.5% to 5%.[2] However the synthesis of PC$_{61}$BM, PC$_{71}$BM and other emerging low band gap polymers are potentially problematic due to their total energy requirements emanating from numerous low yielding synthetic steps and inefficient purification procedures.[3,4] The need for active materials with less demanding synthetic routes and therefore lower embedded energy is required. For this technology to become a commercial and environmental success it is important that we apply the 12 principles of "green chemistry"/sustainable chemical processes.[5–7] The development of more sustainable replacements for PC$_{61}$BM should address several of the green chemistry principles, for example, prevent waste, maximize atom economy,

[a] Address here. a University of Toronto, Department of Chemical Engineering & Applied Chemistry, 200 College Street, Toronto, Ontario, Canada. M5S 3E5.
[b] Department of Chemistry, University of Toronto, 80 St. George Street, Toronto, Ontario, Canada, M5S 3H6
[c] Department of Chemical and Biological Engineering, University of Ottawa 161 Louis Pasteur Pvt., Ottawa, Canada, K1N 6N5
[d] Department of Materials Science and Engineering, University of Toronto, 184 College Street, Toronto, Ontario, Canada M5S 3E4
†These two authors contributed equally to the experimental aspects of this article.
*Correspondence to be made to benoit.lessard@uottawa.ca (B.H.L.) and tim.bender@utoronto.ca (T.P.B.)
Electronic Supplementary Information (ESI) available.

View Article Online
DOI: 10.1039/C6TA10739G




design less hazardous synthesis, the reduction of derivatives/intermediates and the maximization of energy efficiency resulting in minimized embedded energy.[5–7]

In addition to using starting materials that require less energy intensive synthesis, how the devices themselves are built and processed can also aid in the overall devices performance. Engineering parameters such as thermal annealing, choice of solvent, weight ratios of donor to acceptor, and the use of an electroactive solid additives have been reported to enhance the PCE for P3HT:$PC_{61}$BM BHJ OPV devices.[8–17] So called ternary BHJs are generically comprised of three photoactive and/or electroactive components resulting in greater device efficiencies while maintaining comparable device fabrication ease.[8–10,14,15]

For a ternary additive to be effective, they must produce a cascade charge transfer effect between the P3HT and $PC_{61}$BM by acting as intermediate donor/acceptors.[8] Additionally, a ternary additive should increase the light absorption of the OPV and contribute to additional photocurrent production at wavelengths of light not absorbed by P3HT and $PC_{61}$BM (e.g.: 450-650 nm).

A solid ternary additive that has recently received renewed interest is silicon phthalocyanine (SiPc).[18–20] Metal/metalloid containing phthalocyanines (MPcs) are molecules which classically have been applied as industrial pigments and dyes, due to their strong optical properties and general chemical stability. Compared to other active materials, such as $PC_{61}$BM, MPcs require on average 2-orders of magnitude less energy to synthesize and purify.[3,4] Recently, MPcs have found application as the photoactive layer in planar heterojunction (PHJ) OPVs,[21–2324] organic light emitting diodes (OLEDs)[25] and organic thin film transistors (OTFTs).[26–28] Unlike more common MPcs, such as copper and zinc, SiPc contains a tetravalent metal that can form two axial bonds perpendicular to the phthalocyanine chromophore.[29–31] This enables a chemical handle for the tuning of both physical and electrical properties. We have shown for example that the position and frequency of fluorine atoms within fluoro phenoxy SiPcs influences such factors in PHJ OPVs.[31]

The sum of favourable frontier orbitals, absorption in the 650-700 nm range and chemically addressable axial substituents have been shown to make SiPcs promising candidates as ternary additives in BHJ OPVs.[32,33] Honda *et al.* first established in a number of studies the use of bis(tri-*n*-hexylsilyl oxide) SiPc ($(3HS)_2$-SiPc, **Figure 1**) as an electronically active ternary additive in BHJ OPV devices.[33–36] The addition of as little as 4 wt% $(3HS)_2$-SiPc to a P3HT:$PC_{61}$BM BHJ OPV was found to increase the device PCE by up to 20%.[33] Honda *et al.* determined that $(3HS)_2$-SiPc was found mostly at the P3HT:$PC_{61}$BM interface and that the increased efficiency from the additive arose not only from the increased photo charge generation from the SiPc chromophore absorbance (at 700 nm), but also due to increased electron transfer from P3HT to $PC_{61}$BM due to the fore mentioned cascading effect.[36] $(3HS)_2$-SiPc has also been chemically modified to comprise tert-butyl groups on the SiPc aromatic periphery,[37,38] and has then been used in ternary BHJ OPV devices or even used in combination with other additives such as indene-$C_{60}$ bisadduct (ICBA) in quaternary BHJ OPV devices.[39] Honda *et al.*[34] as well as others[40–42] have also explored the use of bis(tri-*n*-hexylsilyl oxide) functionalized silicon naphthalocyanine (SiNc) based additives to take advantage of the increased photo charge generation at 750-850 nm corresponding to the dyes respective absorbance.

Our group recently completed a follow up study to that of Honda *et al.*, where we explored the use of various phthalocyanine and subphthalocyanine compounds as solid additives in P3HT:$PC_{61}$BM BHJ OPV devices to determine if they would perform in a similar manner to $(3HS)_2$-SiPc.[32] Consistent with the results from Honda *et al.*, we observed an increase in device efficiency of up to 20% for devices incorporating $(3HS)_2$-SiPc as an additive. Furthermore, our study found that $(3HS)_2$-SiPc outperformed all other additives, such as bis(tri-*n*-hexylsilyl oxide) germanium phthalocyanine ($(3HS)_2$-GePc) and tri-*n*-hexylsilyl oxide boron subphthalocyanine ((3HS)-BsubPc). While working with $(3HS)_2$-SiPc, we observed that the compound had an extreme tendency to crystallize while also being highly soluble – contradictory properties. We hypothesized that the unique combination of high solubility and a seemingly strong driving force to crystallize were in part responsible for the improved OPV device efficiency described by Honda *et al*.[29]

Following up on these findings, we decided to synthesize a series of chemical variants of $(3HS)_2$-SiPc to determine if the crystallinity and solubility could be altered, and to determine if this would result in increased performance in BHJ OPV devices therefore forming a structure property relationship. In this study, we explore two structural variants to $(3HS)_2$-SiPc and determine their potential roles in BHJ OPV devices as solid additives. Also based on their HOMO/LUMO energy levels and our previous experiences with SiPcs as electron acceptors, we for the first time have probed $(3HS)_2$-SiPc and the structural variants as direct $PC_{61}$BM replacements within BHJ OPVs and therefore start to expand their functional potential.

## Experimental

### Materials

All ACS grade solvents were purchased from Caledon Laboratories (Caledon, Ontario, Canada) and used without further purification unless otherwise stated. 1,3-diaminoisoindoline (DI3) was purchased from Xerox Corporation (Mississauga, ON) and used as received. Silicon tetrachloride ($SiCl_4$), 1,2-dichlorobenzene (anhydrous, 99%), and cesium hydroxide (CsOH), were purchased from Sigma Aldrich and used as received. Tri-*n*-hexylchlorosilane (3HS), tri-*n*-butylchlorosilane (3BS), and triisopropylchlorosilane (3TS) were purchased from Gelest (Morrisville, Pennsylvania, USA) and used as received. Dihydroxysilicon phthalocyanine (SiPc-$OH_2$) was synthesized according to the literature.[32]

### Methods

All reactions were performed under an atmosphere of nitrogen gas using oven dried glassware. Ultraviolet-visible (UV-vis) absorption spectra were acquired on a PerkinElmer Lambda 1050 UV / vis / NR spectrometer using a PerkinElmer quartz cuvette with a 10 mm path length. Electrochemical analysis was performed on a BASI C3 cell stand using an Ag / AgCl counter-electrode and a glassy carbon working electrode and a scan rate of 100 mV / s. Samples were dissolved in a 0.1 mol / mL tetrabutyl ammonium perchlorate solution in DCM. The thermal stability of the SiPcs were characterized by thermogravimetric analysis (TGA) using a TA Instrument Q50 and differential scanning calorimetry (DSC) using a TA Instrument Q1000. Thermal decomposition temperature ($T_d$) was obtained by TGA using a heating rate of 10 °C / min and was defined as the temperature at which 5% weight loss of the compounds is observed under nitrogen. DSC was performed on the SiPc derivatives using the following profile: first heat to 275 °C (bellow $T_d$) at a rate of +5 °C / min followed by a first cooling to 0 °C (-5 °C / min), a second heat to 275 °C (+5 °C / min), a flash cooling to 0 °C (-100 °C / min), a third heat to 275 °C (+5 °C / min) and a final

View Article Online
DOI: 10.1039/C6TA10739G




cooling to 0 °C (-5 °C / min). The melting temperature ($T_m$) and enthalpy of melting ($\Delta H_m$) were identified in the second heating run as the onset and the area of the peak in the heat flow versus temperature plots, respectively. The crystallization temperature ($T_c$) and enthalpy of crystallization ($\Delta H_c$) were calculated from the first cooling run as the onset and the area of the peak in the Heat flow versus temperature plots, respectively. The flash crystallization temperature ($T_{cf}$) and associated enthalpy of crystallization ($\Delta H_{cf}$) were identified from the fourth run (second cooling) and quantified similarly to $T_c$ and $\Delta H_c$.

**Chemical Synthesis**

***Bis(tri-n-hexylsilyl oxide) silicon phthalocyanine ((3HS)$_2$-SiPc).*** (3HS)$_2$-SiPc was synthesized according to the literature.[32,43] For example, the synthesis of (3HS)$_2$-SiPc was accomplished by introducing SiPc-OH$_2$ (1.82 g, 3.17 mmol), tri-*n*-hexylchlorosilane (10.1 g, 31.7 mmol) and pyridine (182 mL) in a 250 mL three neck round bottom flask with a reflux condenser and nitrogen inlet. The mixture was stirred and heated at 115 °C under nitrogen for 5 hours, allowed to cool to room temperature and gravity filtered resulting in a purple powder residue. The filtrate was concentrated and precipitated in methanol prior to filtration, yielding a dark blue powder. (Yield = 41%) Analytics were identical to previously reported.[5] Prior to device integration, (3HS)$_2$-SiPc was further purified by vacuum distillation to achieve electronic grade purity.

***Bis(tri-n-butylsilyl oxide) silicon phthalocyanine ((3BS)$_2$-SiPc).*** (3BS)$_2$-SiPc was synthesized and purified using the same method as (3HS)$_2$-SiPc, except reacting SiPc-OH$_2$ (1.22 g, 2.12 mmol) with tri-*n*-butylchlorosilane (5.0 g, 21.2 mmol) in pyridine (112mL), yielding a dark blue powder. (Yield = 43%) HRMS (EI) [M] calcd for 971.46, found 971.5. $^1$H NMR: δ = 9.63 to 9.65 ppm (8H, m), 8.30 to 8.33 ppm (8H, m), 0.10 to 0.01 ppm (30H, m), -1.26 to -1.30 ppm (12H, m) and -2.41 to -2.44 ppm (12H, m).

***Bis(tri-n-isopropylsilyl oxide) silicon phthalocyanine ((3TS)$_2$-SiPc).*** (3TS)$_2$-SiPc was synthesized and purified using the same method as (3HS)$_2$-SiPc, except reacting SiPc-OH$_2$ (1.49 g, 2.59 mmol) with tri-*n*-isopropylchlorosilane (5.0 g, 25.9 mmol) in pyridine (149 mL) for 20h, yielding a dark blue powder. (Yield = 52%) HRMS (EI) [M] calcd for 887.30, found 887.4. $^1$H NMR: δ = 9.62 to 9.65 ppm (8H, m), 8.30 to 8.33 ppm (8H, m) and -1.13 to -1.18 ppm (36H, m) and -2.03 to -2.09 ppm (6H, m).

**Fabrication and characterization of photo voltaic devices**

***Preparation of substrates.*** Indium tin oxide (ITO) coated glass substrates (Colorado Concept Coatings LLC) were rubbed with aqueous detergent followed by ultra-sonication in aqueous detergent, deionized water, acetone, and methanol for 5 minutes each, followed by air plasma treatment for 10 minutes. A thin layer of poly(3,4-ethylenedioxythiophene):poly(styrene sulfonic acid) (PEDOT:PSS, Clevios™ AI 4083) was then spin-coated onto the ITO glass at subsequent speeds of 500 rpm for 10 seconds and 4000rpm for 30 seconds, then dried in air at 115 °C on a hot plate for 15 minutes. All the subsequent steps were performed in the controlled atmosphere in the glove box.

***Preparation of photocells containing ternary blend P3HT:(3XS)$_2$-SiPc:PC$_{61}$BM.*** P3HT, PC$_{61}$BM and the (3XS)$_2$-SiPc derivatives were dissolved in 1,2-dichlorobenzene (ODCB, 40 mg / mL solutions) and were stirred at 50 ˚C overnight to ensure complete dissolution of the solids. The individual solutions were then combined in ratios as required for each device and were stirred again at 50 °C for 3 hours to ensure complete mixing. The photoactive solutions were spin-casted onto the PEDOT:PSS at 600 rpm for 1 minute. The resulting layers were placed in a glass Petri dish with a partially uncovered lid for 20 h. It should be noted that no any thermal treatment was performed in this study. LiF (1 nm) and Al (80 nm) were deposited under high vacuum (~ 1 x 10$^{-7}$ Torr). The resulting ternary solar cell have the following structure: Glass / ITO / PEDOT:PSS / P3HT:(3XS)$_2$-SiPc:PC$_{61}$BM / LiF / Al.

***Preparation of devices containing binary blend P3HT:(3XS)$_2$-SiPc.*** P3HT is first solubilized in 1,2-dichlorobenzene (ODCB) to form a solution with concentration of 20 mg/ml. The solution was heated at 45 °C for 2 hours.. The concentration of (3HS)$_2$-SiPc, (3BS)$_2$-SiPc and (3TS)$_2$-SiPc were 11.8 mg/mL, 11.3 mg/mL and 11 mg/mL, respectively. The resulting solutions were heated at 45 °C overnight. The active layer was created by spin-coating the mixture onto the PEDOT:PSS at 1000 rpm for 1 minute. It should be note that the solution was kept at 45 °C during spin-coating process. Spin-casting the active layer at lower speed of 500 rpm led to the film with the visible crystals at the surface (Fig S2-4, Supporting Information). Also, spin-casting solution at room temperature led to the formation of crystals. Using higher concentration of (3XS)$_2$-SiPc of 16 mg/mL also led to the formation of film with defaults. (See Figure 4S, Supporting information). A thin layer of bathocuproine (BCP) was deposited on the top of the active layer as buffer layer (7 nm). The cells were completed by evaporating 80 nm of Ag as top electrode. The resulting photocells have the following architecture: Glass / ITO / PEDOT:PSS / P3HT:(3XS)$_2$-SiPc / BCP / Ag. The vacuum chamber had a base pressure of ~ 8 x 10$^{-8}$ Torr, and a working pressure ~ 1 x 10$^{-7}$ Torr during deposition of BCP and Ag. Deposition rate was monitored by quartz crystal microbalance (QCM, Inficon) calibrated against films deposited on glass with thicknesses measured by step edge contact profilometry.

***Photovoltaic Characterization of Devices.***

Voltage characteristics and external quantum efficiencies (EQE) were obtained under nitrogen atmosphere using simulated solar light supplied by a 300W Xenon Arc lamp with an Air Mass 1.5 Global filter, fed through a Cornerstone™ 260 1 / 4 m Monochromator with a Keithley 2401 Low Voltage SourceMeter. Wavelength scans of the devices were performed and corresponding currents measured using a Newport Optical Power Meter 2936-R controlled by TracQ Basic software and the light intensity was calibrated with reference to a UV-silicon photodetector. Each device contained five pixels and the error bars found in all device plots and tables correspond to an average of these pixels. The surface of the active layer is 20 mm$^2$.

## Results and discussion

**Chemical, Optical and Electrochemical Characterization of (3XS)$_2$-SiPc derivatives**

Wheeler *et al.* first synthesized (3HS)$_2$-SiPc by converting silicon phthalocyanine dichloride ((Cl)$_2$-SiPc) into silicon phthalocyanine dihydroxide ((OH)$_2$-SiPc) which was then coupled using chloro tri-n-hexylsilane through simply refluxing in pyridine for 5 h (**Scheme 1**).[43] The formation of (OH)$_2$-SiPc can be performed with negligible losses in yield however the coupling with tri-n-hexylsilane itself gave a total yield of roughly 53%. Since then Gessner *et al.*

View Article Online
DOI: 10.1039/C6TA10739G




successfully synthesized $(3HS)_2$-SiPc by directly reacting $(Cl)_2$-SiPc with chloro tri-n-hexylsilane under reflux in chlorobenzene for a few hours using Aliquat® HTA-l (trioctyl methyl ammonium chloride), a phase transfer catalyst. This procedure resulted in an improved yield of as much as 93%.[44] In this study we chose to avoid the use of Aliquat® HTA-l due to its inevitable presence in the final product and the difficulty associated to its necessary removal prior to integration into sensitive organic electronic devices. Honda et al.[33–35] and Flora et al. [45] used $(3HS)_2$-SiPc which was purchased from Aldrich, and based on publication date we surmise it was synthesized using the method described in the Wheeler *et al.* study.

We have previously described our synthetic protocol for $(3HS)_2$-SiPc (**Figure 1**) which follows the Wheeler method.[32,43] The procedure was replicated to synthesize the two chemical variants bis(tri-*n*-butylsilyl oxide) SiPc ($(3BS)_2$-SiPc, **Figure 1**) and bis(tri-*n*-isopropylsilyl oxide) SiPc ($(3TS)_2$-SiPc, **Figure 1**). See the experimental section for details on the synthesis and analysis. This relatively high yielding synthesis requires no formation of derivatives/intermediates, contains no hazardous reagents, produces little waste and is only 3-steps: characteristics that are in line with the 12 principles of "green chemistry"/sustainable chemical processes.

Once purified, the compounds were characterized by UV-vis absorbance spectroscopy in toluene and the resulting characteristic spectra can be found in **Figure 2A**. The energy gap ($E_{GAP,Opt}$) associated to each SiPc derivative was calculated using, $E_{GAP,Opt} = c*h/\lambda_{onset}$, where $c$ = the speed of light, $h$ = Plank's constant and $\lambda_{onset}$ is taken as the onset of the absorption spectra for each compound. The maximum absorbance ($\lambda_{max}$) and $E_{GAP,Opt}$ are outlined in **Table 1**. As expected, it was found that all three compounds absorb in the same wavelength range at 600-700 nm and have nearly identical $E_{GAP,Opt}$ all consistent with previous studies by our group[31,32] and others[43,46,47].

Electrochemical analysis was performed on both $(3BS)_2$-SiPc and $(3TS)_2$-SiPc and compared to previously obtained values for $(3HS)_2$-SiPc (**Figure 2**).[32] From the measured half wave potentials, the highest occupied molecular orbital (HOMO) and lowest unoccupied molecular orbital (LUMO) energy levels can be estimated using empirical correlations.[48–51] Again, as expected, the three SiPc derivatives have similar electrochemical properties (**Table 1**). No significant changes in photo- or electro-physical properties were therefore observed due to the variation of functional groups from n-hexyl to n-butyl to isopropyl.

**Baseline P3HT:$PC_{61}$BM BHJ OPV Devices**

A series of baseline BHJ OPV devices, where the active layer was a 1.0:0.8 mixture of P3HT:$PC_{61}$BM, were repeatedly fabricated throughout the study and used as a point of comparison. The devices were found to have an average $J_{SC}$ = 8.8 mA/cm$^2$, $V_{OC}$ = 0.55 V, *FF* = 0.60, and *PCE* = 2.90% (averaged over 6 sets of device runs, each run had a total of 3-4 cells). These results are consistent with efficiencies reported by our group and others.[2,25]

**P3HT:$PC_{61}$BM:$(3XS)_2$-SiPc ternary BHJ OPV Devices**

As mentioned in the introduction, Honda *et al.* previously established that the addition of small amount of $(3HS)_2$-SiPc (3.7% in weight) to a P3HT:$PC_{61}$BM BHJ OPV resulted in significant increases in $J_{SC}$.[33] In our previous study, we explored the use of different MPcs as ternary additives and found that none were as effective as $(3HS)_2$-SiPc.[32] We again replicated our devices with 3.7 wt% $(3HS)_2$-SiPc as a ternary additive and similar to the previously reported results,[32,33] we were able to achieve a device PCE of ~3.3%.

Following this set of devices, we then explored the use of $(3BS)_2$-SiPc and $(3TS)_2$-SiPc in place of $(3HS)_2$-SiPc. It was observed that the use of both $(3BS)_2$-SiPc and $(3TS)_2$-SiPc as a ternary additive resulted in a further but modest increase in $J_{SC}$ of roughly ~10% when compared to $(3HS)_2$-SiPc, while maintaining the increase in $V_{OC}$ and subsequently a higher efficiency (**Figure 3A**). The pronounced secondary peak in the EQE at 700 nm confirms that these compounds are also contributing to photogeneration (**Figure 3B**). Additionally, the increase in the EQE spectrum in the primary range (300-600 nm) indicates that $(3BS)_2$-SiPc and $(3TS)_2$-SiPc are enabling a further increase in efficiency via the cascade electron transfer from P3HT to $PC_{61}$BM as when using $(3HS)_2$-SiPc. This increase in EQE over the entire spectra as well as the simultaneous increase in $J_{SC}$ and $V_{OC}$ suggests that the SiPc derivatives are in fact at the interface. When the additive is miscible in the P3HT or the $PC_{61}$BM phase we would expect a drop in $V_{OC}$ and increase in $J_{SC}$.[12,13] Corresponding metrics are tabulated in **Table 2**.

We performed 2D and 3D tapping-mode atomic force microscopy (AFM, surface area: 5 × 5 μm$^2$) on films of P3HT:$PC_{61}$BM blends incorporating various $(3XS)_2$-SiPc (**Figure 4**). The image of the P3HT:$PC_{61}$BM blends cast from ODCB in the absence of $(3XS)_2$-SiPc (**Figure 4A**) reveals coarse chain-like features, which is typical for the mixture of P3HT:$PC_{61}$BM. The root-means square (RMS) roughness of P3HT:$PC_{61}$BM was found to be 8.45 nm. The blend films incorporating $(3XS)_2$-SiPc (3.7% in weight) showed a rougher surface relative to that of P3HT:$PC_{61}$BM. A RMS roughness of 13.1 nm and 12.9 nm was measured for $(3HS)_2$-SiPc and $(3TS)_2$-SiPc respectively. The highest RMS was found for the mixtures incorporating $(3BS)_2$-SiPc of 17.7 nm. Rougher actives surface layers can provide a rougher metal–polymer interface, which can be desirable for efficient charge collection through a larger surface area.[52] The morphology of the three ternary systems (topography and phase) shows the similarity, the presence of $(3XS)_2$-SiPc as solid additives alter the morphology of the blend, which is showed in AFM images in phase (**Figure 5**). This demonstrates that the three $(3XS)_2$-SiPcs induce a change in nanomorpholoy of the resulting blend in the same way. These results further suggest that an additional phase is not formed and that the morphology of the P3HT:$PC_{61}$BM binary mixture is preserved.

**P3HT:$(3XS)_2$-SiPc binary BHJ OPV devices**

As previously mentioned above, we have demonstrated the application of SiPcs as electron accepting layers in PHJ OPVs when paired with electron donor materials such as α-sexithiophene.[22,53–56] To the best of our knowledge, the use of SiPcs as a sole electron accepting material in place of $PC_{61}$BM in BHJ OPV devices has not yet been reported. As we have found in our previous studied and outlined herein, $(3HS)_2$-SiPc and its analogs have an odd mix of high solubility and the high tendency to crystallize. We therefore explored the hypothesis that they may be able to substitute $PC_{61}$BM in a solution processed BHJ OPV device. In an attempt to compare directly against our baseline P3HT:$PC_{61}$BM, the ratio of P3HT:$(3XS)_2$-SiPc of 1:0.8 and the concentration of P3HT of 20 mg/mL was used initially. However, the resulting films where highly defective with crystals formed large enough to see visually (**Figure S5**, Supporting Information). Therefore, we decreased the concentration to 11 mg/mL and the resulting films were suitable to make functional devices.

The photovoltaic performance of devices containing P3HT as donor and $(3XS)_2$-SiPc as acceptor are tabulated in **Table 3**.

View Article Online
DOI: 10.1039/C6TA10739G




Compared to the P3HT:$PC_{61}BM$ baseline device, the P3HT:$(3XS)_2$-SiPc devices gave a higher $V_{OC}$, while even though a substantially reduced *Jsc* limited their overall efficiency. The best performances have been obtained for devices prepared with $(3TS)_2$-SiPc as acceptor, resulting from higher $V_{OC}$ and $J_{SC}$.

**Figure 6B** shows the external quantum efficiency (EQE) of binary devices. Compared to the P3HT:$PC_{61}BM$ devices, an EQE peak at 700 nm was observed, which corresponds to the absorbance of SiPc (**Figure 6C**), suggesting indicating that the $(3XS)_2$-SiPc does in fact contribute to photogeneration. These results illustrate that SiPc can act as electron acceptor molecules in fullerene-free BHJ OPV devices. The devices composed of P3HT and $(3TS)_2$-SiPc showed the highest EQE, resulting to the highest current density. The UV-Vis absorption of the P3HT:$(3XS)_2$-SiPc films show similar features. The absorption of film containing P3HT:$(3TS)_2$-SiPc exhibits a slight redshift as compared to those of P3HT:$(3HS)_2$-SiPc and P3HT:$(3BS)_2$-SiPc which is comparable to the EQE spectrum, but the reason is not clear. AFM was used to identify a possible reason for the improved performance of P3HT:$(3TS)_2$-SiPc and P3HT:$(3BS)_2$-SiPc over P3HT:$(3HS)_2$-SiPc. **Figure 7A** elucidates the topology and the phase images of P3HT:$(3HS)_2$-SiPc films. Significant phase separation took place as evidence by the relatively large domains which were formed on the microscale size (1 µm × 0.500 µm). We determined the RMS roughness = 21.2 nm. When using $(3BS)_2$-SiPc we observed smaller square domains on the order of 150 nm (**Figure 7B**), and when using $(3TS)_2$-SiPc no significant crystal were identified (**Figure 7C**). Thin films prepared using $(3BS)_2$-SiPc and $(3TS)_2$-SiPc exhibit smoothers surfaces compared to $(3HS)_2$-SiPc with RMS = 12.9 nm and 9.43 nm, respectively. These results suggest that smaller domain sizes afforded by the use of $(3BS)_2$-SiPc and $(3TS)_2$-SiPc could be the reason for their improved performance over $(3HS)_2$-SiPc.

While these device efficiencies are not record-breaking it is important to note that they show tremendous promise. This is the first report of their use in OPVs which suggest a great deal of improvement in device performance can be expected through future molecular design and device optimization. Secondly, it is well known that the synthesis of $PC_{61}BM$ and other low band gap polymers are extremely energy intensive due to the numerous complex synthetic steps and low yielding purifications.[3,4] Phthalocyanines, however, require a fraction of the energy to synthesize and purify due to the limited required synthetic steps and straight forward purification procedures. For example, Anctil *et al.* have shown zinc phthalocyanine and copper phthalocyanine require 70-120 times less energy to produce than $PC_{61}BM$ and 105-173 times less energy to produce than $PC_{71}BM$.[3,4] These findings suggest that while SiPc derivatives are not yet outperforming $PC_{61}BM$, they do merit further investigation. This leads to the question of direction in molecular design and engineering of $(3XS)_2$-SiPcs.

**X-ray diffraction (XRD) of $(3XS)_2$-SiPc single crystals.**

For reference, during our previous study, large single crystals of $(3HS)_2$-SiPc were grown by slow evaporation from pyridine and diffracted by X-ray crystallography,[32] and had comparable solid state arrangements to other soluble SiPc derivatives.[57] While synthesizing and purifying $(3BS)_2$-SiPc we found that, similar to $(3HS)_2$-SiPc, the compound had a strong tendency to crystalize. Crystals of $(3BS)_2$-SiPc (CCDC#: 1522758) were also grown by the same method, and displayed a similar crystal packing motif and crystal densities to $(3HS)_2$-SiPc.[32,51,58] **Figure 8** illustrates the characteristic solid state arrangements of both $(3BS)_2$-SiPc and $(3HS)_2$-SiPc. Each compound has similar π-π stacking arrangements with only a slight change in overall density of 1.204 g/mol and 1.251 g/mol for $(3HS)_2$-SiPc and $(3BS)_2$-SiPc respectively. The single crystal diffraction of $(3TS)_2$-SiPc proved to be less straightforward. Very large (apparent) crystals, often in the mm range, were grown from various techniques, such as evaporation from pyridine, vapour diffusion of heptane into THF and others (pictures of some of the specimens can be found in the supporting information, **Figure S6**). In all cases, these exceptionally large (apparent) crystals would crumble rather than split into pieces and no characteristic X-ray diffractions could be obtained from any of the fractions. In addition to frustrating the X-ray crystallographer, these observations suggest that these molecules may not pack periodically. Therefore, the solid state arrangements could not be characterized for $(3TS)_2$-SiPc. These results represent the beginning of a structure property relationship and as our groups develop additional families of SiPc derivatives we will be able to more clearly correlate the crystal diffraction patterns to OPV performance.

**X-ray diffraction (XRD) of the thin solid films**

X-ray diffraction (XRD) was performed on spun cast thin solid films of both P3HT:$(3XS)_2$-SiPc binary mixtures and P3HT:$PC_{61}BM$:$(3XS)_2$-SiPc ternary mixtures (**Figure 9A**). The concentrations, compositions and spin rates used were identical to those used to make the respective BHJ OPV devices found in **Table 3**. All films experienced a primary diffraction peak at 2θ = 5.46° which corresponds to the d-spacing of P3HT at ($d$ = 1.62 nm).[59,60] For the P3HT:$PC_{61}BM$ films only the primary peak for P3HT was observed with no significant peaks associated to $PC_{61}BM$. This has been well reported and understood as neat films of $PC_{61}BM$ are known to be amorphous.[37] However, under the same conditions, when substituting the $PC_{61}BM$ for a $(3XS)_2$-SiPcs, a secondary sharp crystalline diffraction is observed in the XRD patterns. In all films (**Figure 9A**) the P3HT diffraction is roughly the same intensity while the intensity of SiPc changes with chemical structure. For example, $(3HS)_2$-SiPc exhibits a diffraction, with a larger $d$ = 1.32 nm compared to $(3BS)_2$-SiPc, where $d$ = 0.99 nm and $(3TS)_2$-SiPc, $d$ = 1.03 nm (**Figure 9B**). The fwhm (full width half max) of $(3HS)_2$-SiPc (0.21°) and $(3BS)_2$-SiPc the (0.19°) are very small and much smaller than P3HT (1.04°), indicating strong $(3XS)_2$-SiPc crystalline domains even when mixed with P3HT. These results are consistent with the idea that $(3HS)_2$-SiPc has a strong driving force for crystallization.[32] These results are interesting when compared to the OPV device performance: $(3BS)_2$-SiPc and $(3TS)_2$-SiPc were characterized by having higher density crystallites (smaller d-spacing) compared to $(3HS)_2$-SiPc and both resulted in increased device efficiency as a ternary additive or as a PCBM substitute. We surmise that the tendency to form larger crystallites may be the reason $(3HS)_2$-SiPc is underperforming compared to the new derivatives. That being said, **Figure 9B** illustrates the XRD patterns of P3HT:$P_{61}BM$:$(3XS)_2$-SiPc ternary films. None of the ternary mixtures exhibited the sharp crystalline peaks observed in the binary mixture. While it is likely that at this loading (3.7 wt%) the signal is too weak to observe, Oku *et al.* have hypothesized that the absence of peak is in fact indication that the SiPc molecules are at the P3HT:$PC_{61}BM$ interfaces.[37] In all cases the P3HT diffraction is similar and no peaks corresponding to the SiPc was observed, suggesting that the overall P3HT:$PC_{61}BM$ crystallinity is preserved regardless of the $(3XS)_2$-SiPc additive.

**Thermal characterization**

View Article Online
DOI: 10.1039/C6TA10739G




Using thermogravimetric analysis (TGA), the thermal decomposition temperature ($T_d$) was obtained for all three SiPc derivatives (**Figure S1**). In all cases, similar degradation profiles were obtained, resulting in $T_d$ = 318 °C, 342 °C and 375 °C for $(3BS)_2$-SiPc, $(3HS)_2$-SiPc and $(3TS)_2$-SiPc respectively (**Figure 10**). In attempts to gain a better insight into the melting and crystallization characteristics of these SiPc molecules differential scanning calorimetry (DSC) was used to characterize all three SiPc derivatives resulting in the identification of the melting temperature ($T_m$), enthalpy of melting ($\Delta H_m$), crystallization temperature ($T_c$) and enthalpy of crystallization ($\Delta H_c$) were calculated from the heat flow versus temperature plots represented in **Figure 10** and can be found in **Table 4**.

For $(3HS)_2$-SiPc a single transition was observed between 0 °C and 275 °C, where $T_c < T_m$ and $\Delta H_c \approx \Delta H_m$, which is consistent with a common undercooling effect. $(3BS)_2$-SiPc appears to have two similar and distinct transitions consistent with two melt / crystalize transitions (**Figure 10**, **Table 4**). The first transition (≈ 60 °C) experienced a smaller $\Delta H_c \approx \Delta H_m \approx$ 26 J / g while the second transition (≈ 220-230 °C) has a greater $\Delta H_c \approx \Delta H_m \approx$ 31-36 J / g. In contrast, $(3TS)_2$-SiPc had no discernable transitions between 0 °C and 275 °C, which is perhaps consistent with the fact that it is not diffractable material as outlined above. It is important to note that even when flash cooling the samples (-100 °C / min) the same transitions were observed, albeit at slightly lower temperatures, which is expected with the increase in cooling rate (**Table 4**). The DSC results confirm that both $(3BS)_2$-SiPc and $(3HS)_2$-SiPc have a thermodynamic tendency to crystalize at both slow and fast cooling rates, while the kinetics of nucleation growth is will admittedly dependent on the system. This confirms our original hypothesis for $(3HS)_2$-SiPc. It also perhaps begins to form some design rules around the molecular design for these types of SiPcs for the applications outlined herein. Further analysis into nucleation rates and processing conditions would be required to fully quantify the tendency to crystalize from a solution of organic solvent, P3HT and $PC_{61}BM$. As mentioned above, these results represent the beginning of a structure property relationship and with the further development of SiPc derivatives we likely will be able to correlate thermal characterization with XRD and OPV performance.

## Conclusions

In this study we have confirmed our previous result that the use of $(3HS)_2$-SiPc as a ternary additive in P3HT:$PC_{61}BM$ BHJ OPV device can achieve efficiencies of up to 3.3%. We then synthesized two chemical variants of $(3HS)_2$-SiPc (trihexyl), namely $(3BS)_2$-SiPc (tributyl) and $(3TS)_2$-SiPc (triisopropyl), and explored their chemical properties along with their performance in BHJ OPV devices as electron acceptors in fullerene-free BHJs and as solid ternary additives in P3HT:$PC_{61}BM$:$(3XS)_2$-SiPc BHJ OPV devices. No significant change in their respective UV-Vis absorption spectrum or electrochemical analysis was observed between $(3TS)_2$-SiPc, $(3BS)_2$-SiPc and $(3HS)_2$-SiPc.

When incorporated as ternary additives in P3HT:$PC_{61}BM$:$(3XS)_2$-SiPc BHJ OPV devices, both $(3BS)_2$-SiPc and $(3TS)_2$-SiPc resulted in a further increase in *Jsc* of roughly ~10% when compared to using $(3HS)_2$-SiPc, and subsequently a higher efficiency. In a similar result to the use of $(3HS)_2$-SiPc, the pronounced secondary peak in the EQE at 700 nm confirms that these compounds are contributing to photogeneration. In addition, the improvement in devices performance is resulted from the enhance morphology.

Secondly, binary P3HT:$(3XS)_2$-SiPc BHJ OPV devices using $(3HS)_2$-SiPc, $(3BS)_2$-SiPc, and $(3TS)_2$-SiPc achieving efficiencies of 0.25% and 0.78% and 1.07% respectively. An increase in $V_{OC}$ over the P3HT:$PC_{61}BM$ baseline devices was observed, and despite the relatively low overall efficiencies this result exemplifies the potential for SiPc as an electron acceptor in solution processed BHJ OPV devices. It is also important to note that $(3BS)_2$-SiPc and $(3TS)_2$-SiPc outperforms $(3HS)_2$-SiPc as acceptors and as an additive. It is also important to note that phthalocyanine, such as these SiPc derivatives, require 2-orders of magnitude less energy to synthesize compared to $PC_{61}BM$ due to the limited required synthetic steps and the straight forward purification procedures. These findings suggest that while SiPc derivatives are not yet outperforming $PC_{61}BM$, their use merits further investigation as a greener sustainable alternative overall to $PC_{61}BM$.

XRD of the resulting devices exhibited a consistent and characteristic signal corresponding to P3HT in all the binary and ternary devices. In the binary devices, we see a second sharp and intense peak corresponding to $(3XS)_2$-SiPc. The peaks indicate that $(3XS)_2$-SiPc has a tendency to crystalize even when blended with P3HT. Maybe even more interesting the d-spacing suggests that $(3BS)_2$-SiPc and $(3TS)_2$-SiPc have higher density crystallites (smaller d-spacing) compared to $(3HS)_2$-SiPc. Therefore, we surmise that the tendency to form smaller crystallites may be the reason $(3BS)_2$-SiPc and $(3TS)_2$-SiPc are superior additives to $(3HS)_2$-SiPc. Thermogravimetric analysis confirmed that both $(3BS)_2$-SiPc and $(3HS)_2$-SiPc have a thermodynamic tendency to crystalize at both slow and fast cooling rates.

The results from this study suggest that solubility and driving force to crystalize are important factors in determining the extent to which an additive will migrate to the donor/acceptor interface and thus increase device performance. However, it is currently unclear as to exactly how the crystallization affects the migration of the additive to the interface. Future work will be conducted to build a larger library of SiPc derivatives in attempt to better understand what structural fragments and chemical properties are responsible for improving the performance of a certain $(3XS)_2$-SiPc for BHJ OPV application(s).

## Acknowledgements

This work was supported by a Natural Sciences and Engineer Research Council (NSERC) Banting Post-Doctoral fellowship to BHL and a Discovery Grant to TPB.

## Notes and references

‡ Pictures of $(3TS)_2$-SiPc crystals grown by various techniques, thermo gravimetric analysis (TGA) obtained from powders of $(3XS)_2$-SiPc and photographs of the thin film composed of P3HTand $(3XS)_2$-SiPc can be found in the ESI.

(1) Hoppe, H.; Sariciftci, N. S. Organic solar cells: An overview. *J. Mater. Res.* **2004**, *19* (7), 1924–1945.
(2) Dang, M. T.; Hirsch, L.; Wantz, G. P3HT:PCBM, Best Seller in Polymer Photovoltaic Research. *Adv. Mater.* **2011**, *23* (31), 3597–3602.
(3) Anctil, A.; Babbitt, C. W.; Ra, R. P.; Landi, B. J. Material and Energy Intensity of Fullerene Production. *Environ. Sci. Tech.* **2011**, No. 45, 2353–2359.
(4) Anctil, A.; Babbitt, C. W.; Raffaelle, R. P.; Landi, B. J. Cumulative energy demand for small molecule and polymer photovoltaics. *Prog. Photovoltaics Res.* **2013**, No. July 2012, 1541–1554.

View Article Online
DOI: 10.1039/C6TA10739G




(5) Anastas, P. T.; Williamson, T. C. *Green chemistry: frontiers in benign chemical syntheses and processes*; Oxford University Press: USA, 1998.
(6) Namies, J. Trends in Analytical chemistry The 12 principles of green analytical chemistry and the SIGNIFICANCE mnemonic of green analytical practices. **2013**, *50*, 78–84.
(7) Kerton, F. M.; Marriott, R.; Kraus, G. *Alternative Solvents for Green Chemistry*, 2nd ed.; Kraus, G., Ed.; RSC green chemistry series; Royal Society of Chemistry: Cambridge, UK, 2013.
(8) Yang, L.; Yan, L.; You, W. Organic solar cells beyond one pair of donor-acceptor: Ternary blends and more. *J. Phys. Chem. Lett.* **2013**, *4* (11), 1802–1810.
(9) Chen, Y.-C.; Hsu, C.-Y.; Lin, R. Y.-Y.; Ho, K.-C.; Lin, J. T. Materials for the Active Layer of Organic Photovoltaics: Ternary Solar Cell Approach. *ChemSusChem* **2013**, *6* (1), 20–35.
(10) Ameri, T.; Khoram, P.; Min, J.; Brabec, C. J. Organic ternary solar cells: A review. *Adv. Mater.* **2013**, *25* (31), 4245–4266.
(11) Chen, M. C.; Liaw, D. J.; Huang, Y. C.; Wu, H. Y.; Tai, Y. Improving the efficiency of organic solar cell with a novel ambipolar polymer to form ternary cascade structure. *Sol. Energy Mater. Sol. Cells* **2011**, *95* (9), 2621–2627.
(12) Street, R. A.; Davies, D.; Khlyabich, P. P.; Burkhart, B.; Thompson, B. C. Origin of the Tunable Open-Circuit Voltage in Ternary Blend Bulk Heterojunction Organic Solar Cells. *J. Am. Chem. Soc.* **2013**, *135* (3), 986–989.
(13) Khlyabich, P. P.; Burkhart, B.; Thompson, B. C. Efficient Ternary Blend Bulk Heterojunction Solar Cells with Tunable Open-Circuit Voltage. *J. Am. Chem. Soc.* **2011**, *133* (37), 14534–14537.
(14) Dang, M. T.; Hirsch, L.; Wantz, G.; Wuest, J. D. Controlling the Morphology and Performance of Bulk Heterojunctions in Solar Cells. Lessons Learned from the Benchmark Poly(3-hexylthiophene):[6,6]-Phenyl-C61-butyric Acid Methyl Ester System. *Chem. Rev.* **2013**, *113* (5), 3734–3765.
(15) Goubard, F.; Wantz, G. Ternary blends for polymer bulk heterojunction solar cells. *Polym. Int.* **2014**, *63* (8), 1362–1367.
(16) Lu, L.; Chen, W.; Xu, T.; Yu, L. High-performance ternary blend polymer solar cells involving both energy transfer and hole relay processes. *Nat. Commun.* **2015**, *6*, 7327.
(17) Lu, L.; Xu, T.; Chen, W.; Landry, E. S.; Yu, L. Ternary blend polymer solar cells with enhanced power conversion efficiency. *Nat. Photonics* **2014**, *7327*, 1–7.
(18) Ke, L.; Gasparini, N.; Min, J.; Zhang, H.; Adam, M.; Rechberger, S.; Forberich, K.; Zhang, C.; Spiecker, E.; Tykwinski, R. R.; et al. Panchromatic ternary/quaternary polymer/fullerene BHJ solar cells, based on novel silicon naphthalocyanine and silicon phthalocyanine dye sensitizers. *J. Mater. Chem. A* **2016**.
(19) Ke, L.; Min, J.; Adam, M.; Gasparini, N.; Hou, Y.; Perea, J. D.; Chen, W.; Zhang, H.; Fladischer, S.; Sale, A.; et al. A Series of Pyrene-Substituted Silicon Phthalocyanines as Near-IR Sensitizers in Organic Ternary Solar Cells. *Adv. Energy Mater.* **2016**, No. 6, 1502355.
(20) Grant, T. M.; Gorisse, T.; Dautel, O. J.; Wantz, G.; Lessard, B. H. Multifunctional ternary additive in bulk heterojunction OPV: increased device performance and stability. *J. Mater. Chem. A* **2017**, *5*, 1581–1587.
(21) Lessard, B. H.; Mohammad, A. L. A.; Grant, T. M.; White, R.; Lu, Z.-H.; Bender, T. P.; AL-Amar, M.; Grant, T. M.; White, R.; Lu, Z.-H.; et al. From chloro to fluoro, expanding the role of aluminum phthalocyanine in organic photovoltaic devices. *J. Mater. Chem.* **2015**, *3* (9), 5047–5053.
(22) Lessard, B. H.; White, R. T.; AL-Amar, M.; Plint, T.; Castrucci, J. S.; Josey, D. S.; Lu, Z.-H.; Bender, T. P. Assessing the Potential Roles of Silicon and Germanium Phthalocyanines in Planar Heterojunction Organic Photovoltaic Devices and How Pentafluoro Phenoxylation Can Enhance π–π Interactions and Device Performance. *ACS Appl. Mater. Interfaces* **2015**, *7* (9), 5076–5088.
(23) Williams, G.; Sutty, S.; Klenkler, R.; Aziz, H. Renewed interest in metal phthalocyanine donors for small molecule organic solar cells. *Sol. Energy Mater. Sol. Cells* **2014**, *124*, 217–226.
(24) Kim, I.; Haverinen, H. M.; Wang, Z.; Madakuni, S.; Kim, Y.; Li, J.; Jabbour, G. E. Efficient organic solar cells based on planar metallophthalocyanines. *Chem. Mater.* **2009**, *21* (18), 4256–4260.
(25) Plint, T.; Lessard, B. H.; Bender, T. P. Assessing the potential of group 13 and 14 metal/metalloid phthalocyanines as hole transporting layers in organic light emitting diodes. *J. Appl. phys.* **2016**, *119* (1), 145502.
(26) Melville, O.; Lessard, B. H.; Bender, T. P. Phthalocyanine Based Organic Thin-Film Transistors: A Review of Recent Advances. *ACS Appl. Mater. Interfaces* **2015**, *7* (24), 13105–13118.
(27) Kumar, B.; Kaushik, B. K.; Negi, Y. S. Organic Thin Film Transistors: Structures, Models, Materials, Fabrication, and Applications: A Review. *Polym. Rev.* **2014**, *54* (1), 33–111.
(28) Liao, C.; Yan, F. Organic Semiconductors in Organic Thin-Film Transistor-Based Chemical and Biological Sensors. *Polym. Rev.* **2013**, *53* (3), 352–406.
(29) Yamamoto, Y.; Yoshino, K.; Inuishi, Y.; Ichimura, S. Electrical conduction in silicon and germanium phthalocyanine. *Phys. Stat. Sol.* **1980**, *59* (1), 305–310.
(30) Maree, M. D.; Nyokong, T.; Suhling, K.; Phillps, D. Effects of axial ligands on the photophysical properties of silicon octaphenoxyphthalocyanine. *J. Porphyrins Phthalocyanines* **2002**, *6* (6), 373–376.
(31) Lessard, B. H.; Grant, T. M.; White, R.; Thibau, E.; Lu, Z.-H.; Bender, T. P. The position and frequency of fluorine atoms changes the electron donor/acceptor properties of fluorophenoxy silicon phthalocyanines within organic photovoltaic devices. *J. Mater. Chem. A* **2015**, *3*, 24512–24524.
(32) Lessard, B. H.; Dang, J. D.; Grant, T. M.; Gao, D.; Seferos, D. S.; Bender, T. P. Bis(tri-n-hexylsilyl oxide) Silicon Phthalocyanine: A Unique Additive in Ternary Bulk Heterojunction Organic Photovoltaic Devices. *ACS Appl. Mater. Interfaces* **2014**, *6*, 15040–15051.
(33) Honda, S.; Nogami, T.; Ohkita, H.; Benten, H.; Ito, S. Improvement of the Light-Harvesting Efficiency in Polymer/Fullerene Bulk Heterojunction Solar Cells by Interfacial Dye Modification. *ACS Appl. Mater. Interfaces* **2009**, *1* (4), 804–810.
(34) Honda, S.; Ohkita, H.; Benten, H.; Ito, S. Multi-colored dye sensitization of polymer/fullerene bulk heterojunction solar cells. *Chem. Commun.* **2010**, *46* (35), 6596–6598.
(35) Honda, S.; Ohkita, H.; Benten, H.; Ito, S. Selective Dye Loading at the Heterojunction in Polymer/Fullerene Solar Cells. *Adv. Energy Mater.* **2011**, *1* (4), 588–598.
(36) Honda, S.; Yokoya, S.; Ohkita, H.; Benten, H.; Ito, S. Light-Harvesting Mechanism in Polymer/Fullerene/Dye Ternary Blends Studied by Transient Absorption Spectroscopy. *J. Phys. Chem. C* **2011**, *115* (22), 11306–11317.
(37) Oku, T.; Hori, S.; Suzuki, A.; Akiyama, T.; Yamasaki, Y. Fabrication and characterization of PCBM:P3HT:silicon phthalocyanine bulk heterojunction solar cells with inverted structures. *Jpn. J. Appl. Phys.* **2014**, *53* (05FJ08), 1–5.
(38) Lim, B.; Margulis, G. Y.; Yum, J.-H.; Unger, E. L.; Hardin, B. E.; Graetzel, M.; McGehee, M. D.; Sellinger, A. Silicon-Naphthalo/Phthalocyanine-Hybrid Sensitizer for Efficient Red Response in Dye-Sensitized Solar Cells. *Org. Lett.* **2013**, *15* (4), 784–787.
(39) Xu, H.; Ohkita, H.; Benten, H.; Ito, S. Open-circuit voltage of ternary blend polymer solar cells. *Jpn. J. Appl. Phys.* **2014**, *53* (01AB10), 1–4.
(40) Oku, T.; Nose, S.; Yoshida, K.; Suzuki, A.; Akiyama, T.; Yamasaki, Y. Fabrication and characterization of silicon naphthalocyanine, gallium phthalocyanine and fullerene-based organic solar cells with inverted structures. *J. Phys.: Conf. Ser.* **2013**, *433* (1), 12025.
(41) Yoshida, K.; Oku, T.; Suzuki, A.; Akiyama, T.; Yamasaki, Y. Fabrication and Characterization of PCBM : P3HT Bulk Heterojunction Solar Cells Doped with Germanium Phthalocyanine or Germanium Naphthalocyanine. *Jpn. J. Appl. Phys.* **2013**, *53* (05FJ08), 1–5.
(42) Lim, B.; Bloking, J. T.; Ponec, A.; Mcgehee, M. D.; Sellinger, A. Ternary Bulk Heterojunction Solar Cells: Addition of Soluble Nir Dyes for Photocurrent Generation Beyond 800 Nm. **2014**, *6*, 6905–

View Article Online
DOI: 10.1039/C6TA10739G


6913.
(43) Wheeler, B. L.; Nagasubramanian, G.; Bard, A. J.; Schechtman, L. A.; Kenney, M. E. A silicon phthalocyanine and a silicon naphthalocyanine: synthesis, electrochemistry, and electrogenerated chemiluminescence. *J. Am. Chem. Soc.* **1984**, *106* (24), 7404–7410.
(44) Gessner, T.; De, H.; Sens, R.; Ahlers, W.; Vamvakaris, C. Preperation of silicon phthalocyanines and germanium phthalocyanines and related substances. 0113767 A1, 2010.
(45) Flora, W. H.; Hall, H. K.; Armstrong, N. R. Guest emission processes in doped organic light-emitting diodes: Use of phthalocyanine and naphthalocyanine near-IR dopants. *J. Phys. Chem. B* **2003**, *107* (5), 1142–1150.
(46) Chen, H. Z.; Wang, M.; Yang, S. L. Synthesis and photoconductivity study of phthalocyanine polymers. V. 4,4′-diamino-diphenyl ether bridged polymeric SiPc. *J. Polym. Sci. A*. 1997, pp 91–95.
(47) Çoşut, B.; Yeşilot, S.; Durmuş, M.; Kiliç, A.; Ahsen, V. Synthesis and properties of axially-phenoxycyclotriphosphazenyl substituted silicon phthalocyanine. *Polyhedron* **2010**, *29* (2), 675–682.
(48) Noviandri, I.; Brown, K. N.; Fleming, D. S.; Gulyas, P. T.; Lay, P. a; Masters, a F.; Phillips, L. The Decamethylferrocenium/Decamethylferrocene Redox Couple: A Superior Redox Standard to the Ferrocenium/Ferrocene Redox Couple for Studying Solvent Effects on the Thermodynamics of Electron Transfer. *J. Phys. Chem. C* **1999**, *103* (32), 6713–6722.
(49) Li, Y.; Cao, Y.; Gao, J.; Wang, D.; Yu, G.; Heeger, A. J. Electrochemical properties of luminescent polymers and polymer light-emitting electrochemical cells. *Synth. Met.* **1999**, *99* (3), 243–248.
(50) Li, S. G.; Yuan, Z. C.; Yuan, J. Y.; Deng, P.; Zhang, Q.; Sun, B. Q. An expanded isoindigo unit as a new building block for a conjugated polymer leading to high-performance solar cells. *J. Mater. Chem. A* **2014**, *2* (15), 5427–5433.
(51) Sasa, N.; Okada, K.; Nakamura, K.; Okada, S. Synthesis, structural and conformational analysis and chemical properties of phthalocyaninatometal complexes. *J. Mol. Struct.* **1998**, *446* (3), 163–178.
(52) Ma, W.; Yang, C.; Gong, X.; Lee, K.; Heeger, A. Thermally stable, efficient polymer solar cells with nanoscale control of the interpenetrating network morphology. *Adv. Funct. Mater.* **2005**, *15* (10), 1617–1622.
(53) Morse, G. E.; Bender, T. P. Boron subphthalocyanines as organic electronic materials. *ACS Appl. Mater. Interfaces* **2012**, *4* (10), 5055–5068.
(54) Beaumont, N.; Castrucci, J. S.; Sullivan, P.; Morse, G. E.; Paton, A. S.; Lu, Z.-H.; Bender, T. P.; Jones, T. S. Acceptor Properties of Boron Subphthalocyanines in Fullerene Free Photovoltaics. *J. Phys. Chem. C* **2014**, *118* (27), 14813–14823.
(55) Tonzola, C.; Alam, M.; Jenekhe, S. A New Synthetic Route to Soluble Polyquinolines with Tunable Photophysical, Redox, and Electroluminescent Properties. *Macromolecules* **2005**, *38* (23), 9539–9547.
(56) Josey, D. S.; Castrucci, J. S.; Dang, J. D.; Lessard, B. H.; Bender, T. P. Evaluating Thiophene Electron-Donor Layers for the Rapid Assessment of Boron Subphthalocyanines as Electron Acceptors in Organic Photovoltaics: Solution or Vacuum Deposition? *ChemPhysChem* **2015**, *16* (6), 1245–1250.
(57) Lessard, H.; Lough, J.; Bender, T. P. Crystal structures of bis ( phenoxy ) silicon phthalo- cyanines : increasing p – p interactions , solubility and disorder and no halogen bonding observed research communications. *Acta Crystallogr E* **2016**, No. E72, 988–994.
(58) Yang, Y.; Kennedy, V. O.; Updegraph, J. B.; Samas, B.; MacIkenas, D.; Chaloux, B.; Miller, J. a.; Van Goethem, E. M.; Kenney, M. E. Long directional interactions (LDIs) in oligomeric cofacial silicon phthalocyanines and other oligomeric and polymeric cofacial phthalocyanines. *J. Phys. Chem. A* **2012**, *116* (34), 8718–8730.
(59) Kozycz, L. M.; Gao, D.; Hollinger, J.; Seferos, D. S. Donor-Donor Block Copolymers for Ternary Organic Solar Cells. *Macromolecules* **2012**, *45* (14), 5823–5832.
(60) Ong, B. S.; Wu, Y.; Liu, P.; Gardner, S. High-Performance Semiconducting Polythiophenes for Organic Thin-Film Transistors. *J. Am. Chem. Soc* **2004**, *126* (11), 3378–3379.

View Article Online
DOI: 10.1039/C6TA10739G





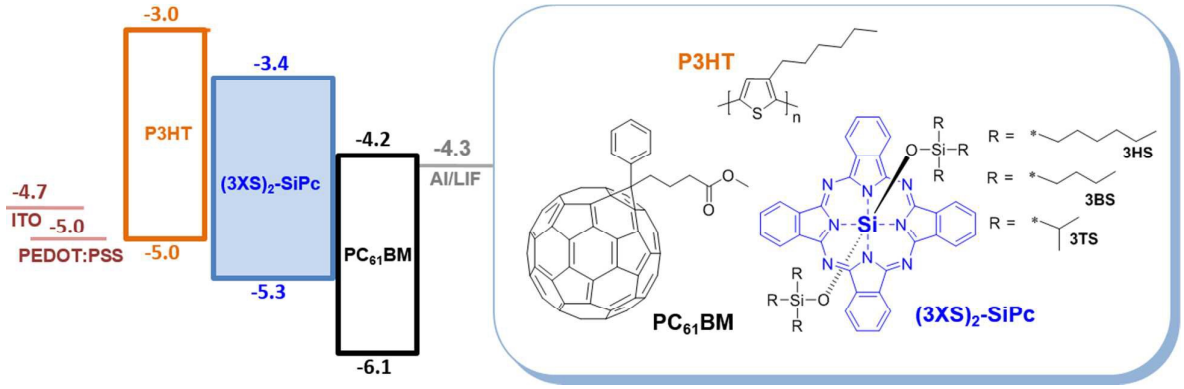


**Figure 1.** Energy level diagram and chemical structure of poly(3-hexylthiophene) (P3HT), bis(tri-n-hexylsilyl oxide) silicon phthalocyanine ($(3HS)_2$-SiPc), bis(tri-n-butylsilyl oxide) silicon phthalocyanine ($(3BS)_2$-SiPc), bis(tri-n-isopropylsilyl oxide) silicon phthalocyanine ($(3TS)_2$-SiPc), and phenyl-$C_{61}$-butyric acid methyl ester ($PC_{61}BM$). The energy levels of the HOMOs and LUMOs were either taken from the literature or derived from electrochemistry (**Table 1**).

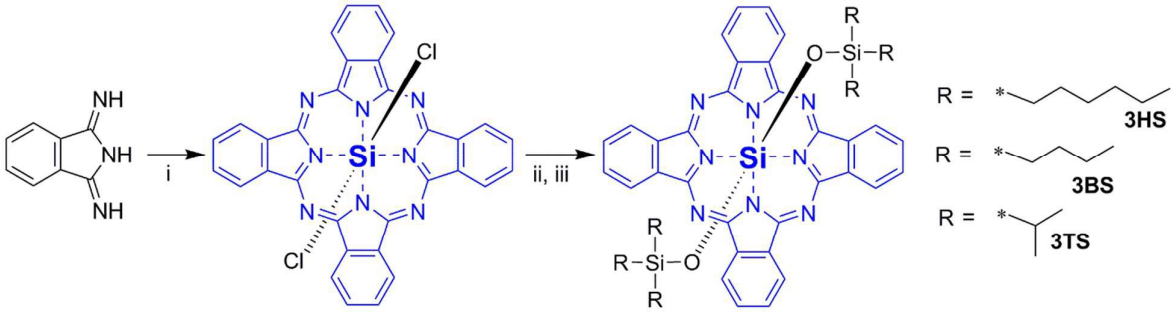


**Scheme 1**. Chemical synthesis scheme for $(3HS)_2$-SiPc, $(3BS)_2$-SiPc or $(3TS)_2$-SiPc, where (i) $SiCl_4$ (1.5 x molar excess), quinoline, 219 ºC, 30 min; (ii) CsOH (50% in water), DMF, 120 °C for 4 h and (iii) chlorosilane derivative ($R_3$-Si-Cl, 5x molar excess), pyridine, 130 °C for 5 h.

View Article Online
DOI: 10.1039/C6TA10739G




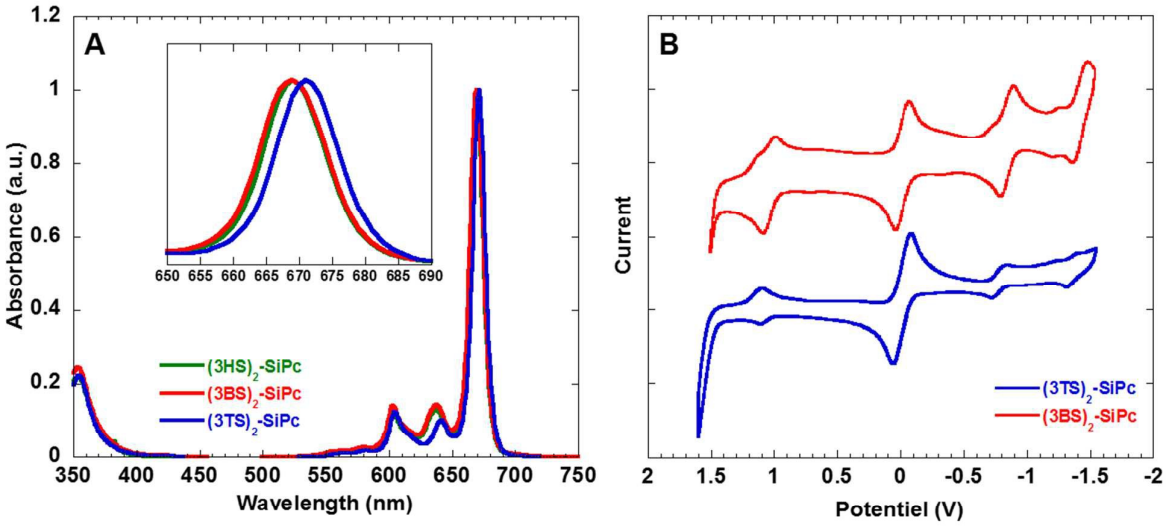


**Figure 2.** A) Normalized UV-vis absorbance and B) Electrochemical spectra for $(3BS)_2$-SiPc and $(3TS)_2$-SiPc. The inset in Figure A is a close up of the scaled absorption peaks between 650 nm and 690 nm. As a comparison, the absorption of $(3HS)_2$-SiPc was added to Figure A.

**Table 1. Electrochemical and UV-vis Characterization of $(3HS)_2$-SiPc, $(3BS)_2$-SiPc, and $(3TS)_2$-SiPc.**

| SiPc derivatives | $E_{RED,1/2}$ (V) | $E_{OX,1/2}$ (V) | $E_{HOMO}$ [a] (eV) | $E_{LUMO}$ [b] (eV) | $\lambda_{max}$ [c] (nm) | $E_{gap,Opt}$ [d] (eV) |
|---|---|---|---|---|---|---|
| $(3HS)_2$-SiPc[e] | -0.85 | 1.04 | -5.31 | -3.42 / -3.49 | 669 | 1.82 |
| $(3BS)_2$-SiPc | -0.84 | 1.04 | -5.31 | -3.43 / -3.49 | 669 | 1.82 |
| $(3TS)_2$-SiPc | -13.4, -0.76 | 1.11 | -5.38 | -3.51 / -3.56 | 671 | 1.82 |

[a] $E_{HOMO} = -(4.27 + E_{OX,1/2})$ eV (scaled to an internal standard of decamethylferrocene)[48–51]
[b] $E_{LUMO,Electro}$ / $E_{LUMO,Opt}$ where $E_{LUMO,Electro} = -(4.27 + E_{Red,1/2})$ and $E_{LUMO,Opt} = E_{Gap,Opt} - E_{HOMO}$
[c] Maximum absorbance, $\lambda_{max}$, of respective compounds dissolved in toluene.
[d] $E_{Gap,Opt}$ determined from the onset of the solution absorbance spectra
[e] The values associated with $(3HS)_2$-SiPc were taken from the literature[32] as a comparison.

View Article Online
DOI: 10.1039/C6TA10739G



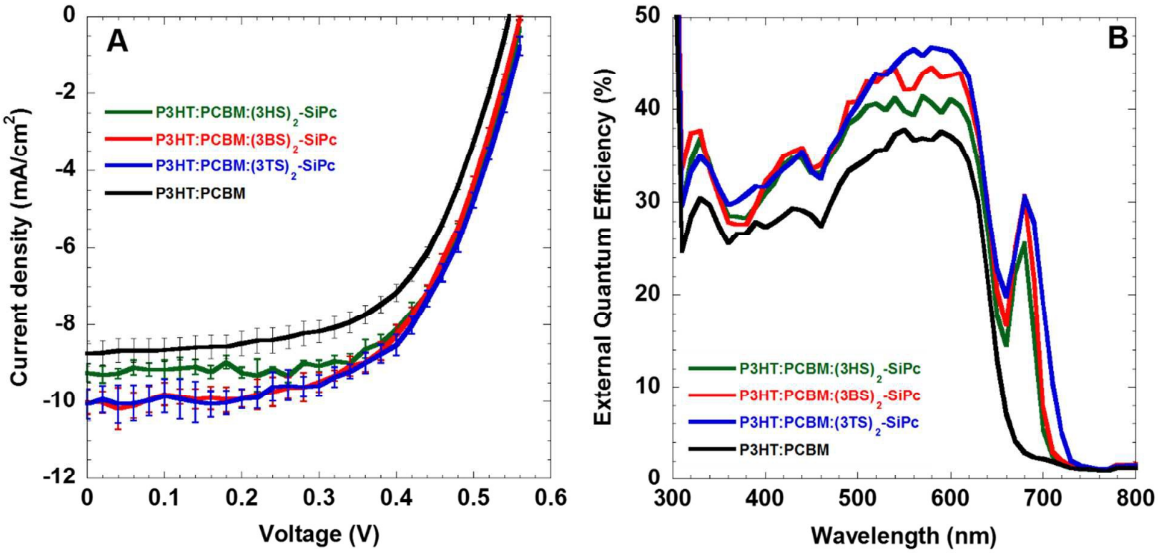


**Figure 3.** A) Characteristic of current density versus voltage (JV) and B) External quantum efficiency (EQE) versus wavelength for device containing P3HT:$PC_{61}BM$:$(3XS)_2$-SiPc (weight ratio: 1.0:0.8:0.07). The error bars in A are the 95% confidence interval of 5-10 devices.

**Table 2.** The photovoltaic performance of P3HT:$PC_{61}BM$ devices incorporating $(3XS)_2$-SiPc as additives.

| ***P3HT:$PC_{61}BM$:X*** [a] | ***Additives*** [b] | $J_{sc}$ (mA / cm$^2$) | $V_{oc}$ (V) | *FF* | *PCE* (%) |
|---|---|---|---|---|---|
| 1:0.8:0 | - | 7.8 ± 0.1 | 0.56 ± 0.01 | 0.60 ± 0.01 | 2.61 ± 0.04 |
| 1:0.8:0.07 | $(3HS)_2$-SiPc | 9.2 ± 0.3 | 0.56 ± 0.01 | 0.63 ± 0.02 | 3.29 ± 0.07 |
| 1:0.8:0.07 | $(3BS)_2$-SiPc | 10.0 ± 0.3 | 0.56 ± 0.01 | 0.59 ± 0.01 | 3.30 ± 0.10 |
| 1:0.8:0.07 | $(3TS)_2$-SiPc | 10.1 ± 0.4 | 0.57 ± 0.01 | 0.60 ± 0.02 | 3.40 ± 0.10 |

a) Mass ratio used to fabricate the active layer of the bulk heterojunction organic photovoltaic (BHJ-OPV) devices, where P3HT represents poly(3-hexylthiophene), $PC_{61}BM$ represents phenyl-$C_{61}$-butyric acid methyl ester and X represents $(3XS)_2$-SiPc = bis(tri-*n*-hexylsilyl oxide) silicon phthalocyanine ($(3HS)_2$-SiPc), bis(tri-*n*-butylsilyl oxide) silicon phthalocyanine ($(3BS)_2$-SiPc) or bis(tri-*n*-isopropylsilyl oxide) silicon phthalocyanine ($(3TS)_2$-SiPc). 1:0.8:0.07 corresponds to a 3.7 wt% loading of $(3XS)_2$-SiPc.

b) identifies which $(3XS)_2$-SiPc was used in the fabrication of the BHJ OPV device.
In all cases experiments the values were averaged with a minimum of 4-5 devices in the case of the P3HT:$PC_{61}BM$ baseline, the values were averaged over a minimum of 46 devices fabricated over the span of 12-16 weeks in the same apparatus. The values were obtained under AM1.5G irradiation at 100 mWcm$^{-2}$.

View Article Online
DOI: 10.1039/C6TA10739G




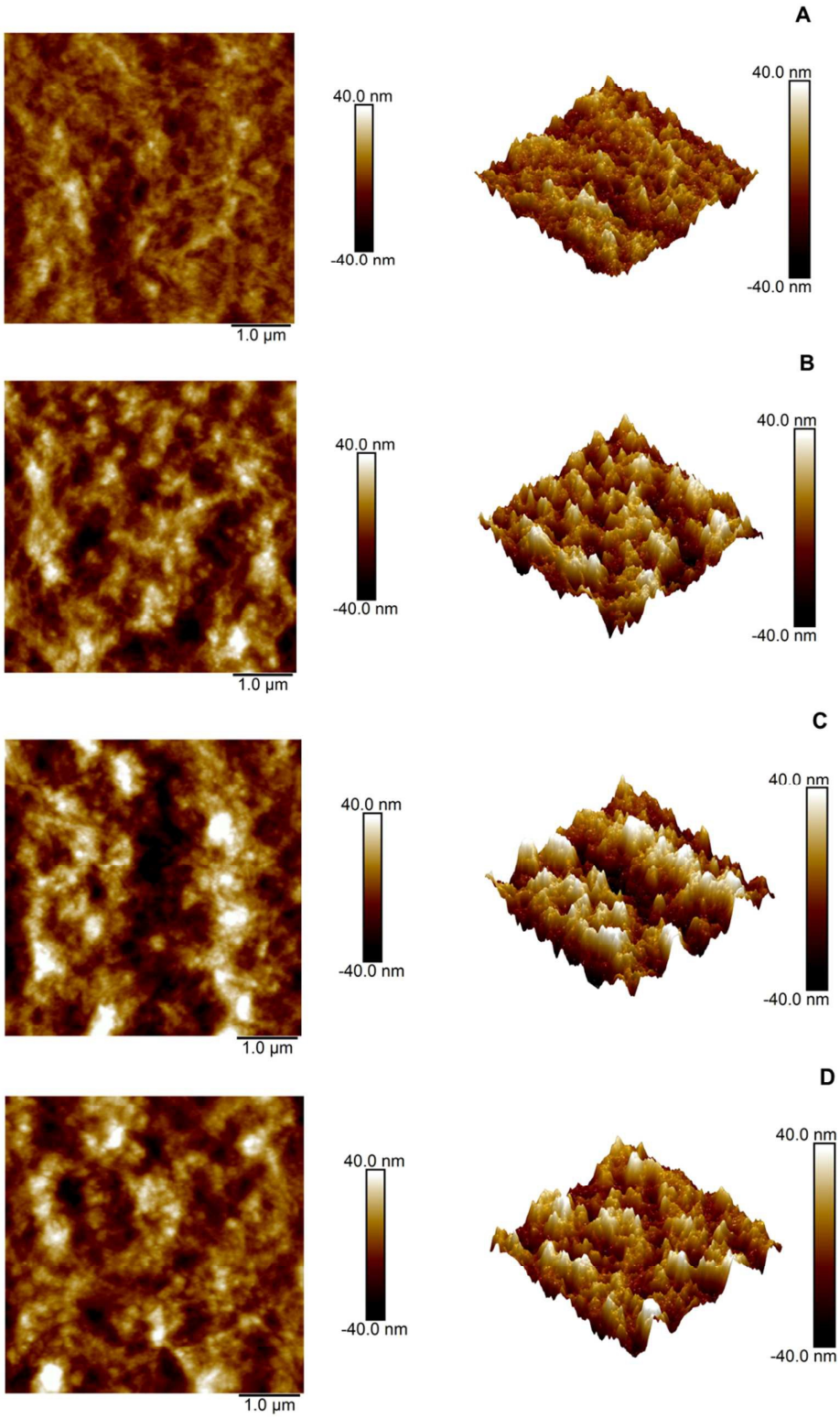


**Figure 4.** Two and three dimensional of topographic AFM images of the surfaces of photoactive layers : A) P3HT:PCBM ($R_{RMS}$ = 8.45 nm), B) P3HT:PCBM:$(3HS)_2$-SiPc ($R_{RMS}$ = 13.1 nm), and C) P3HT:PCBM:$(3BS)_2$-SiPc ($R_{RMS}$ = 17.7 nm), and D) P3HT:PCBM:$(3TS)_2$-SiPc ($R_{RMS}$ = 12.9 nm)

View Article Online
DOI: 10.1039/C6TA10739G



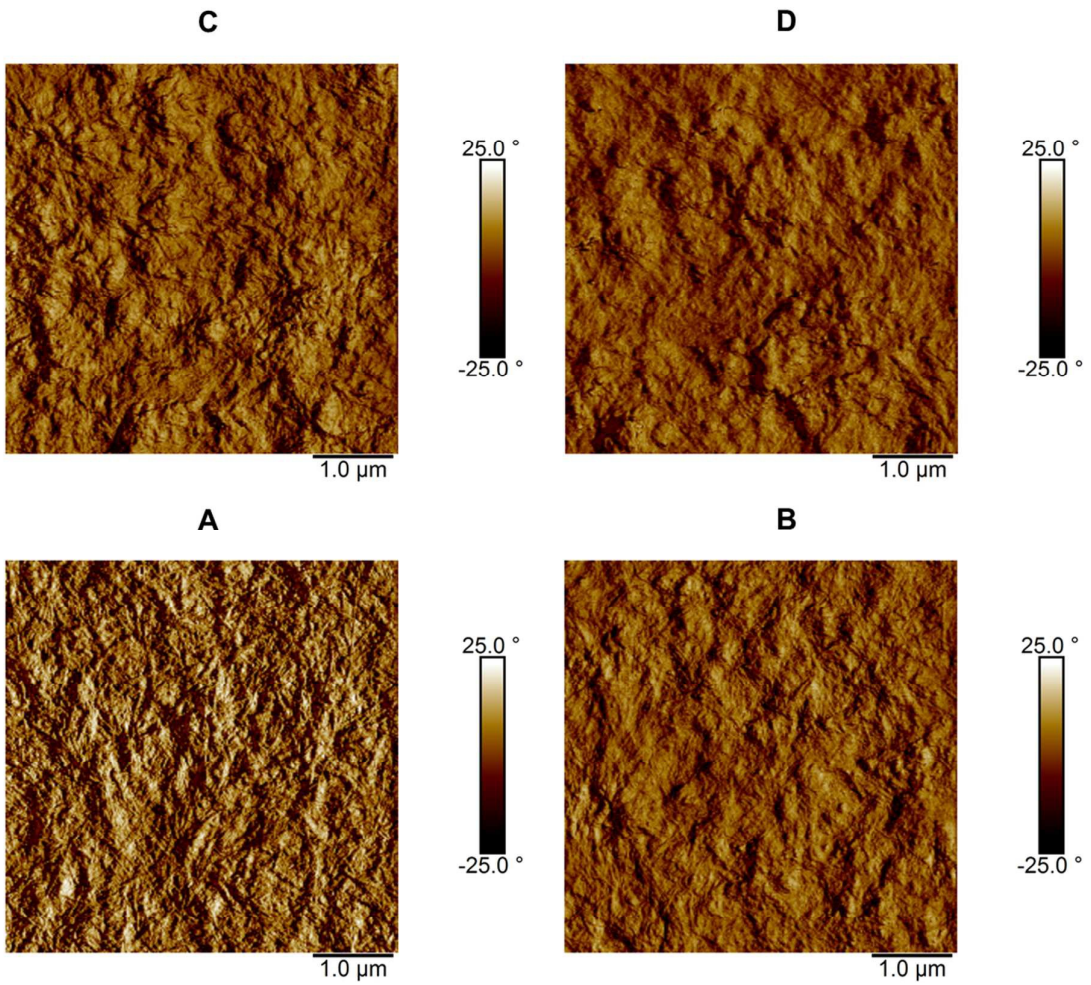


**Figure 5.** AFM phase images of the surfaces of photoactive layers : A) P3HT:PCBM, B) P3HT:PCBM:$(3HS)_2$-SiPc, C) P3HT:PCBM:$(3BS)_2$-SiPc, and D) P3HT:PCBM:$(3TS)_2$-SiPc

View Article Online
DOI: 10.1039/C6TA10739G


**Table 3 The photovoltaic performance of devices containing binary blend P3HT:$(3XS)_2$-SiPc**

| *Donor:Acceptor* | $V_{OC}$ *(V)* | $J_{SC}$ *(mA / cm$^2$)* | *FF* | *PCE (%)* |
|---|---|---|---|---|
| P3HT:$(3HS)_2$-SiPc | 0.70 ± 0.06 | 0.99 ± 0.17 | 0.37 ± 0.02 | 0.25 ± 0.05 |
| P3HT:$(3BS)_2$-SiPc | 0.75 ± 0.03 | 2.61 ± 0.26 | 0.40 ± 0.03 | 0.78 ± 0.07 |
| P3HT:$(3TS)_2$-SiPc | 0.84 ± 0.01 | 3.00 ± 0.18 | 0.43 ± 0.01 | 1.07 ± 0.05 |

a) Bulk heterojunction organic photovoltaic (BHJ-OPV) devices, where P3HT represents Poly(3-hexylthiophene) and $(3XS)_2$-SiPc = bis(tri-*n*-hexylsilyl oxide) silicon phthalocyanine ($(3HS)_2$-SiPc), bis(tri-*n*-butylsilyl oxide) silicon phthalocyanine ($(3BS)_2$-SiPc) or bis(tri-*n*-isopropylsilyl oxide) silicon phthalocyanine ($(3TS)_2$-SiPc). In all cases experiments the values were averaged with a minimum of 4-5 devices obtained under AM1.5G irradiation at 100 mWcm$^{-2}$.

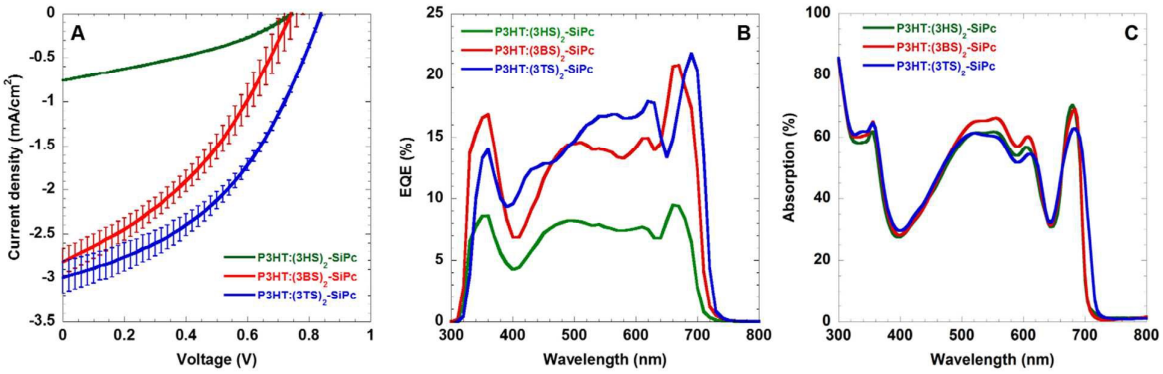


**Figure 6.** (A) Characteristic current density versus voltage (JV); ( B) external quantum efficiency (EQE) versus wavelength, and (C) UV-Vis absorption spectrum of P3HT:$(3XS)_2$-SiPc thin films .

View Article Online
DOI: 10.1039/C6TA10739G





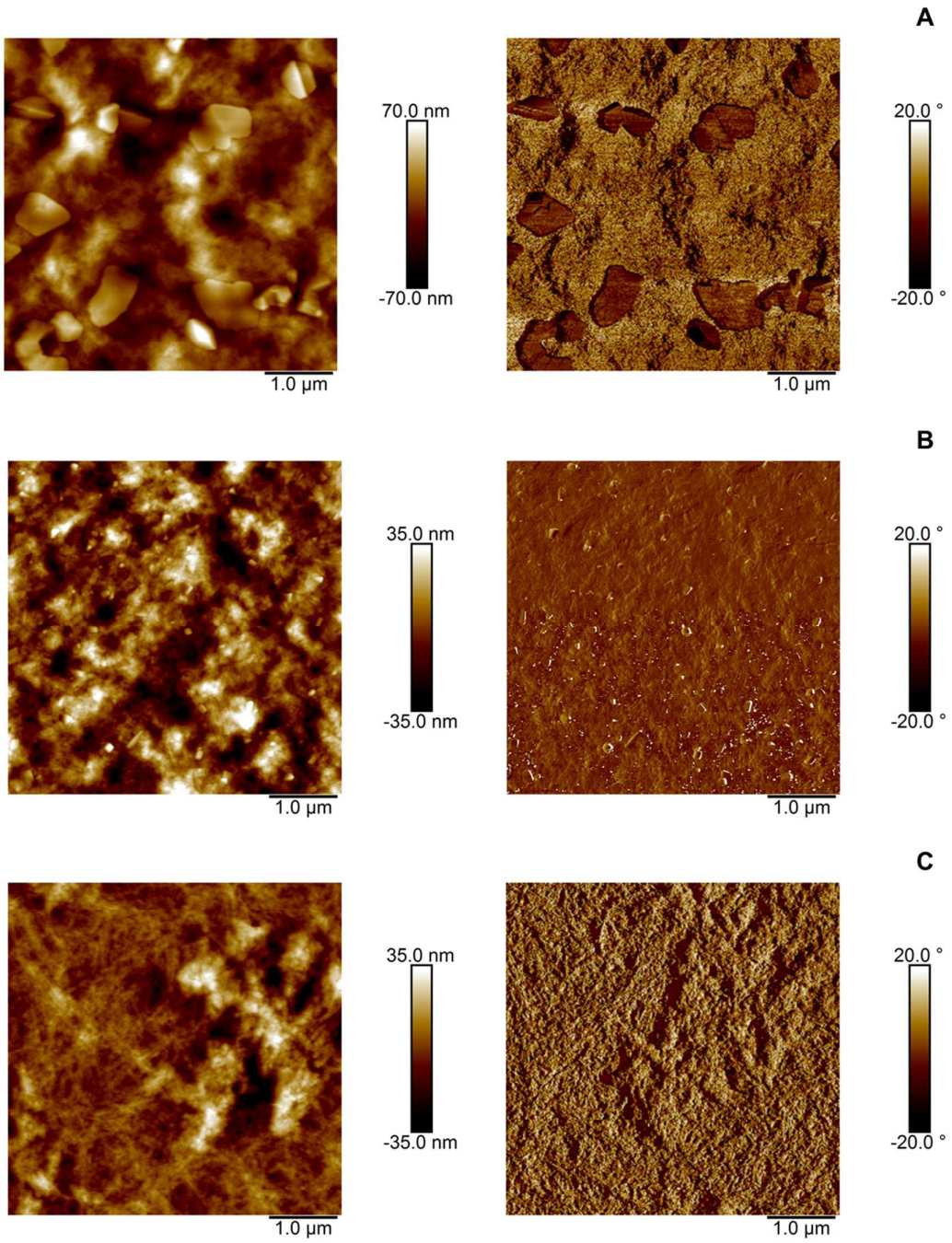


**Figure 7.** Height (left) and phase (right) AFM images of the surfaces of photoactive layers: A) P3HT:$(3HS)_2$-SiPc, B) P3HT:$(3BS)_2$-SiPc, and C) P3HT:$(3TS)_2$-SiPc.

View Article Online
DOI: 10.1039/C6TA10739G


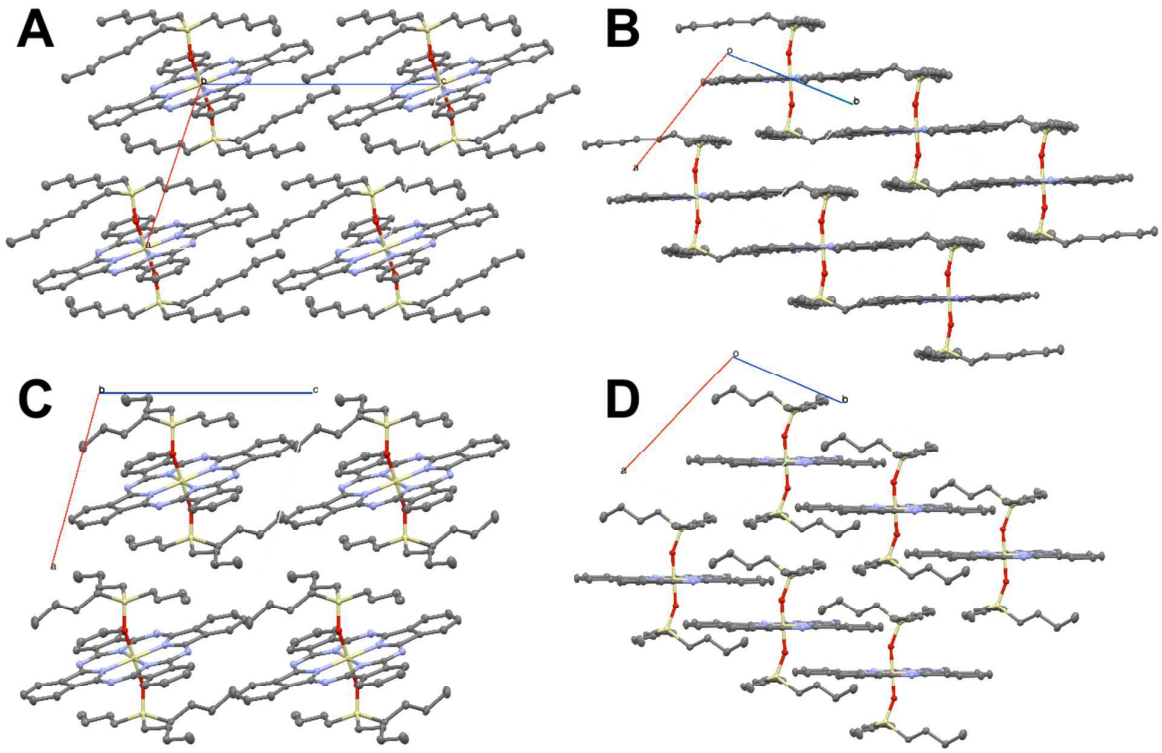


**Figure 8.** Solid state arrangements for $(3HS)_2$-SiPc (A, B)[32,51,58], and for $(3BS)_2$-SiPc (C, D) obtained from X-ray diffraction (CCDC#: 1522758).

View Article Online
DOI: 10.1039/C6TA10739G



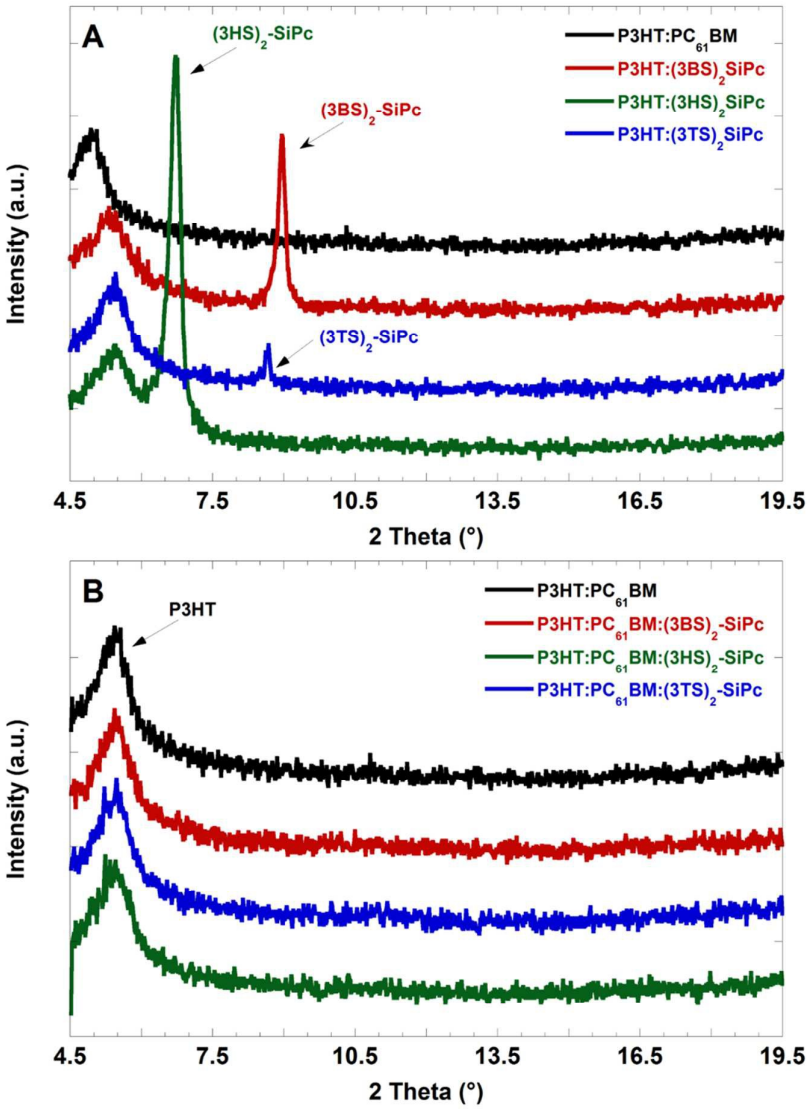


**Figure 9.** Powder X-ray diffraction (XRD) patterns of spun cast thin films of A) P3HT:$(3XS)_2$-SiPc binary mixtures and B) P3HT:$PC_{61}BM$:$(3XS)_2$-SiPc ternary mixtures. The mixture compositions are the same as those used in the BHJ OPV devices represented in Table 2,3.

View Article Online
DOI: 10.1039/C6TA10739G




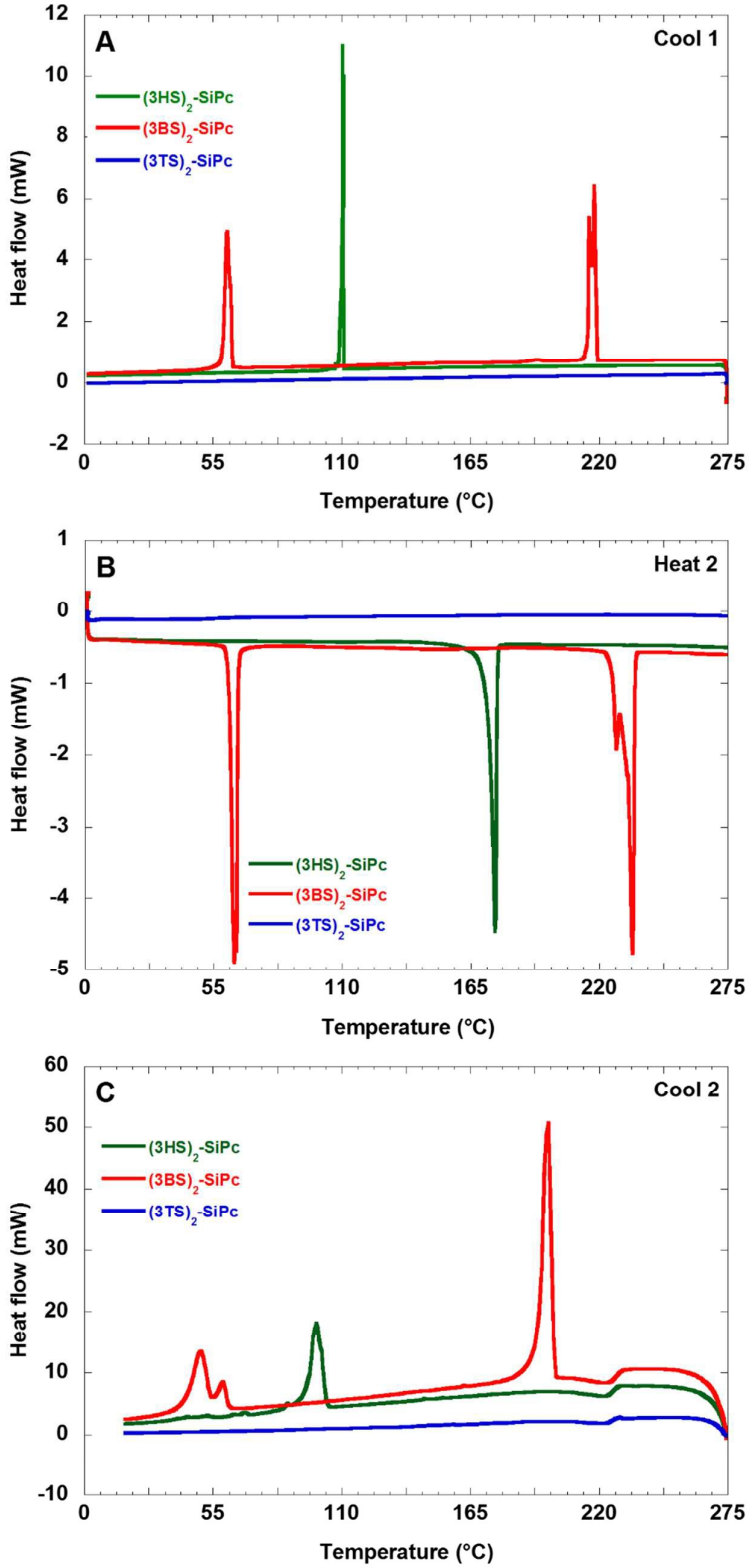


**Figure 10.** Differential scanning calorimetry (DSC) obtained from powders of $(3HS)_2$-SiPc (green), $(3BS)_2$-SiPc (red) and $(3TS)_2$-SiPc (blue). DSC was performed using the following profile: first heat to 275 °C at a rate of +5 °C / min followed by A) a first cooling to 0 °C (-5 °C / min), B) a second heat to 275 °C (+5 °C / min), C) a flash cooling to 0 °C (-100 °C / min), a third heat to 275 °C (not shown, +5 °C / min) and a final cooling to 0 ºC (not shown, -5 °C / min).

View Article Online
DOI: 10.1039/C6TA10739G



**Table 4. Thermodynamic Characterization of $(3HS)_2$-SiPc, $(3BS)_2$-SiPc, and $(3TS)_2$-SiPc**

| SiPc derivatives | $T_d$ [a] (ºC) | $T_m$ [b] (ºC) | $\Delta H_m$ [b] (J / g) | $T_c$ [b] (ºC) | $\Delta H_c$ [b] (J / g) | $T_{cf}$ (ºC) | $\Delta H_{cf}$ (J / g) |
|---|---|---|---|---|---|---|---|
| $(3HS)_2$-SiPc | 342 | 173 | 26.9 | 110 | 23.5 | 103 | 19.9 |
| $(3BS)_2$-SiPc | 318 | 231 / 61 | 36.1 / 25.7 | 219 / 63 | 30.7 / 26.5 | 200 / 54 | 30.6 / 27.7 |
| $(3TS)_2$-SiPc | 375 | - | - | - | - | - | - |

[a] Degradation temperature ($T_d$) was determined at 5% weight loss using thermo-gravimetric analysis (TGA).
[b] Melting temperature ($T_m$) and enthalpy of melting ($\Delta H_m$), and crystallization temperature ($T_c$) and and enthalpy of crystallization ($\Delta H_c$) were obtained from the second heat and second cool, respectively, using differential scanning calorimetry (DSC). Both the heat and cooling runs were performed at 5 °C / min. $T_m$ and $T_c$ are calculated as the onset of melting and of crystallization, respectively. A final run was performed at -100 °C / min and the flash crystallization temperature ($T_{cf}$) and associated enthalpy of crystallization ($\Delta H_{cf}$) were identified.

View Article Online
DOI: 10.1039/C6TA10739G



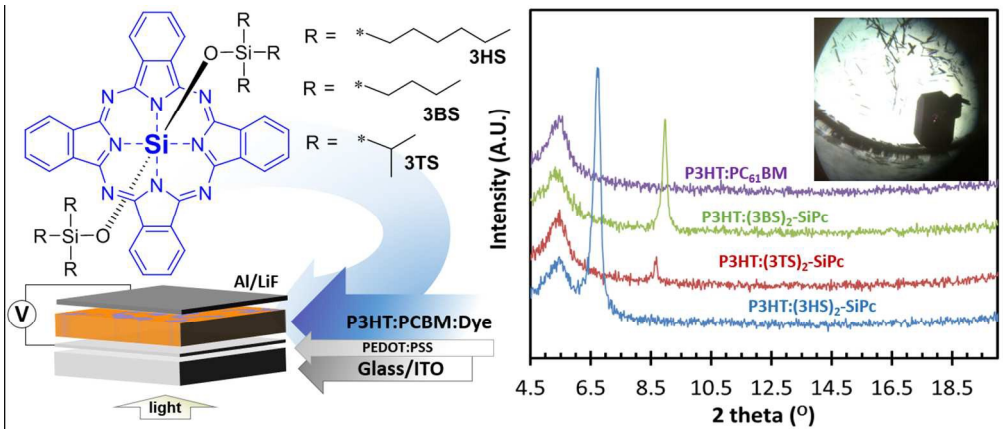


228x96mm (150 x 150 DPI)